Solar Phys (2007) 241: 371–383
DOI 10.1007/s11207-007-0336-1

Periodic Appearance of Coronal Holes and the Related Variation of Solar Wind Parameters

Manuela Temmer · Bojan Vršnak · Astrid M. Veronig

Received: 18 October 2006 / Accepted: 23 January 2007 /
Published online: 30 March 2007

Abstract We compared the variability of coronal hole (CH) areas (determined from daily GOES/SXI images) with solar wind (daily ACE data) and geomagnetic parameters for the time span 25 January 2005 until 11 September 2005 (late declining phase of solar cycle 23). Applying wavelet spectral analysis, a clear 9-day period is found in the CH time series. The GOES/SXI image sequence suggests that this periodic variation is caused by a mutual triangular distribution of CHs $\sim$120° apart in longitude. From solar wind parameters a 9-day periodicity was obtained as well, simultaneously with the 9-day period in the CH area time series. These findings provide strong evidence that the 9-day period in solar wind parameters, showing up as higher harmonic of the solar rotation frequency, is caused by the "periodic" longitudinal distribution of CHs on the Sun recurring for several solar rotations. The shape of the wavelet spectrum from the *Dst* index matches only weakly with that from the CH areas and is more similar to the wavelet spectrum of the solar wind magnetic field magnitude. The distinct 9-day period does not show up in sunspot group areas which gives further evidence that the solar wind modulation is strongly related to CH areas but not to active region complexes. The wavelet power spectra for the whole ACE data range ($\sim$1998 – 2006) suggest that the 9-day period is not a singular phenomenon occurring only during a specific time range close to solar minimum but is occasionally also present during the maximum and decay phase of solar cycle 23. The main periods correspond to the solar rotation (27^{d}) as well as to the second (13.5^{d}) and third (9^{d}) harmonic.

Electronic Supplementary Material The online version of this article (http://dx.doi.org/10.1007/s11207-007-0336-1) contains supplementary material, which is available to authorized users.

M. Temmer (✉) · B. Vršnak
Hvar Observatory, Faculty of Geodesy, Zagreb, Croatia
e-mail: mat@igam.uni-graz.at

B. Vršnak
e-mail: bvrsnak@geodet.geof.hr

A.M. Veronig
IGAM/Institute of Physics, University of Graz, Graz, Austria
e-mail: asv@igam.uni-graz.at

Keywords Coronal holes · Solar wind · Space weather

1. Introduction

Observations of recurrent geomagnetic disturbances with a period of ∼27 days, *i.e.*, corresponding to one solar rotation (so-called Bartels rotation), brought Bartels (1940) to postulate the existence of *M regions* on the Sun as the source of these disturbances. Nowadays these regions are well identified as coronal holes (CHs), characterized by a low density and open magnetic field lines that allow the solar wind as well as energetic particles easily to escape to interplanetary space (*e.g.*, Krieger, Timothy, and Roelof, 1973; Leer, Holzer, and Fla, 1982; Crooker and Cliver, 1994; Fisk, 2005, and references therein). Before the solar minimum, CHs are typically situated at the polar caps with some tongue-like extensions into the equatorial regions, which gives the Sun the appearance of a tilted dipole (Schwenn *et al.*, 2005). The activity belt that is left at the equatorial region is seen as a warped separatrix between positive and negative magnetic field lines that open into interplanetary space carrying an electric current, *i.e.*, the heliospheric current sheet, HCS ("ballerina model" by Alfvén, 1977). As one approaches solar minimum, the HCS loses its warps and becomes flat in close alignment with the solar equatorial plane (Hoeksema, Wilcox, and Scherrer, 1982; Hoeksema, 1995).

Originating from CHs, the high-speed component of the solar wind (high-speed streams, HSSs) is the predominant cause of recurrent geomagnetic storms if they reach the Earth with a southward deflection of the interplanetary magnetic field (Tsurutani and Gonzalez, 1987; Crooker and Cliver, 1994; Tsurutani, Gonzalez, and Guarnieri, 2004). Corotating interaction regions (CIRs; *i.e.*, stable patterns of regions where the slow and fast solar wind interact) in front of HSSs are as well known to substantially contribute to geomagnetic activity owing to the pressure pulse from the compressed plasma (Schwenn, 1983; Crooker and Cliver, 1994; Tsurutani, Gonzalez, and Guarnieri, 2004; Schwenn *et al.*, 2005). The major source of large geomagnetic storms ($Dst \leq -100$ nT) is interplanetary coronal mass ejections (ICMEs) that are earth-directed (Gosling *et al.*, 1991; Tsurutani and Gonzalez, 1997; Cliver and Ling, 2001; Zhang *et al.*, 2003; Alves, Echer, and Gonzalez, 2006). It is reasonable to say that the aforementioned drivers of space weather are closely linked to the structure of the solar corona, hence to the interrelation between active regions and large coronal holes at low latitudes.

The most outstanding period found in solar wind and geomagnetic activity parameters is ∼27 days,[1] *i.e.*, corresponding to one solar rotation. This is not surprising as the solar corona shows a less pronounced differential rotation than the photosphere and a near rigid rotation during minimum activity (*e.g.*, Hoeksema and Scherrer, 1987; Nash, Sheeley, and Wang, 1988; Wang and Sheeley, 1993; Altrock, 2003). Smaller periods of 13.5 as well as 9 and 7 days are also reported (Svalgaard and Wilcox, 1975; Bobova and Stepanian, 1994; Mursula and Zieger, 1996; Neugebauer *et al.*, 2000; Nayar *et al.*, 2001). The 13.5-day period was found predominantly during solar minimum and was therefore assumed to be related to the flat and tilted HCS at this time, which causes an observer at Earth to encounter two high-speed solar wind streams during one solar rotation (Mursula and Zieger, 1996). Bobova and Stepanian (1994) studied geomagnetic data together with solar activity data and suggested that the 13.5-day period is due to variations in the solar chromosphere, such as complexes

[1] All periods stated in the following are synodic periods.

of active regions separated by 180° in longitude (Gaizauskas *et al.*, 1983). However, distinct periodicities of 13.5 days for solar chromospheric variables were found during other phases of the solar cycle as well; thus there might be no causal connection (Mursula and Zieger, 1996). The periodicities of ∼7 and 9 days were associated with the evolution of the warping of the HCS (Nayar *et al.*, 2001).

Vršnak, Temmer, and Veronig (2007) found for a restricted period of low CME activity during 2005, a distinct 9-day period for solar wind parameters and areas of coronal holes. From GOES/SXI images a triangular distribution of three CHs (∼120° apart in longitude) that was stable over several solar rotations was obvious. A stable pattern of CHs might explain in a straightforward manner the obtained periodicities. In the following, we will study common periods in the range 2 – 40 days for solar wind and geomagnetic activity parameters and compare them to the variation of coronal hole areas on the Sun as extracted from GOES/SXI images. Outstanding periods observed for the same time range in CHs and solar wind parameters would enable us to draw direct conclusions on the driver of solar wind variations, namely the occurrence of large CHs. This aim will be achieved by means of wavelet power spectra, which allow us to detect nonstationary periods in the data series and to study their evolution in time.

2. Data Description

Coronal holes are regions of very low density (owing to the escape of the solar wind along open field lines), which makes them to appear as dark features in X-ray images (and EUV). Since December 2004, the Solar X-Ray Imager (SXI) on board the GOES-12 satellite has provided regular observations of the X-ray corona in the wavelength range 6 – 60 Å. As a special data product, coronal hole images are created by stacking 12 hours of solar-rotation-corrected and calibrated X-ray images, which substantially improves the signal-to-noise ratio with respect to individual images (see Hill, Pizzo, and Balch, 2005). From these level-2 files, we chose a data set where continuously daily observations were available. This was the case from 1 January 2005 until 11 September 2005, *i.e.*, day of year (DOY) 1 – 254. This is a time range of low and "simple" solar activity, close to the end of the current cycle no. 23, which is advantageous for our purpose.

We used one SXI level-2 image per day (centered at ∼13 UT) to extract the fractional area of coronal holes that covered the central meridian slice in the longitude range [−10°,10°] (see Figure 1, top panel). For the determination of the CH areas, we applied a fixed threshold to the calibrated SXI coronal hole images of 0.15 DN s^{-1}. All pixels below that threshold (identified as coronal hole pixels) within a specified region of the visible solar disk were summed and divided by the total number of pixels of the considered region to calculate the fractional area covered by CHs. For a more detailed description on the extraction method of the SXI observations see Vršnak, Temmer, and Veronig (2007).

Measurements of the solar wind and interplanetary magnetic field parameters were taken from the Solar Wind Electron, Proton, and Alpha Monitor (SWEPAM; McComas, Bame, and Barker, 1998) and the magnetometer instrument (MAG; Smith, L'Heureux, and Ness, 1998) on board the Advanced Composition Explorer (ACE; Stone, Frandsen, and Mewaldt, 1998). For the analyses we used the daily averages (level-2 data) of the following values: proton density n [cm^{-3}], radial component of proton temperature T [K], proton speed (solar wind (bulk) speed) $|v|$ [km s^{-1}], and the magnetic field magnitude $|B|$ [nT]. The SWEPAM and MAG data were linearly interpolated for days with bad or missing data (total missing data <5%).

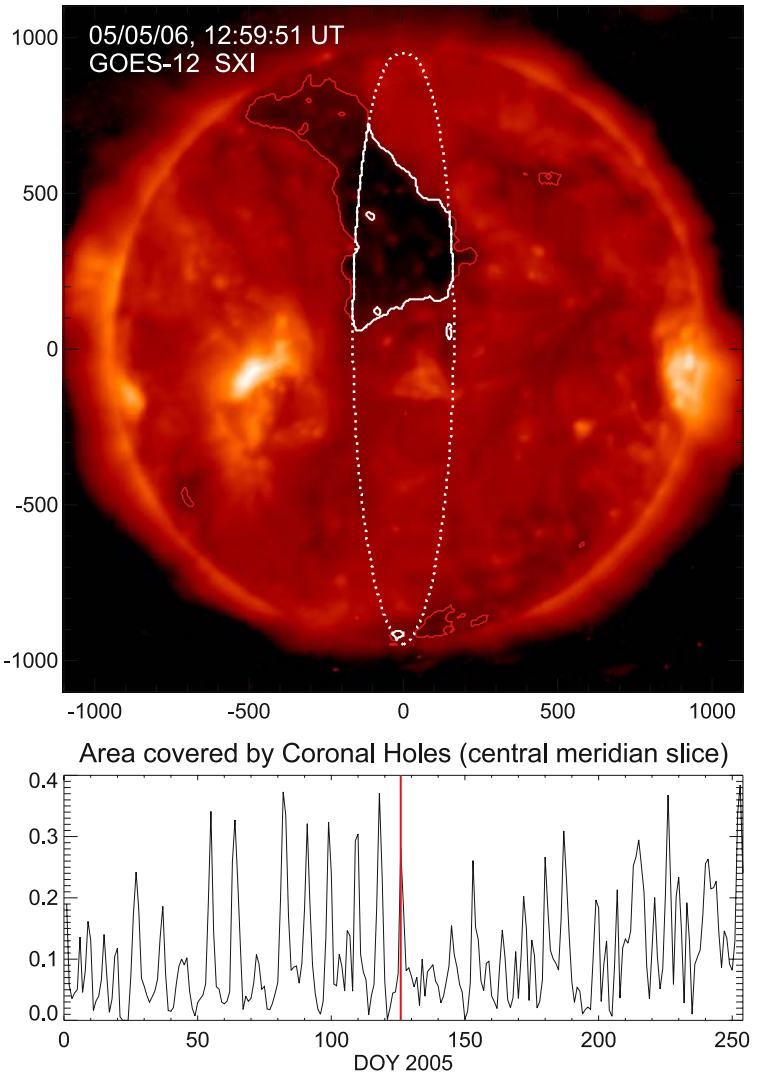

Figure 1 Top: Typical GOES/SXI image from which the fractional CH area within the central meridian slice (white dotted lines) was extracted. The derived CH boundaries are outlined in white (within the measuring slice) and in red (outside the measuring slice). Bottom: Evolution of the fractional CH area in time, given in days of the year (DOY) 2005. The vertical red line indicates the observing date of the image in the top panel. We refer the reader to the online version of Solar Physics for an animation.

As an indicator of the geomagnetic activity we used preliminary daily averages of the disturbance storm time (*Dst*) index (Sugiura and Wilson, 1964) provided by the WDC-2 Kyoto *Dst* index service. The *Dst* index is derived from hourly scalings of horizontal magnetic variations (H component) measured by a network of ground-based low-latitude geomagnetic observatories. The magnitude of the *Dst* index is proportional to the kinetic energy of ring current particles in the Earth magnetosphere, and large negative perturbations are

indicative of geomagnetic storms (Sugiura and Chapman, 1960; Sugiura and Wilson, 1964; Gonzalez, Joselyn, and Kamide, 1994).

As a cross-check regarding possible photospheric causes on the periodic solar wind patterns as suggested in Bobova and Stepanian (1994), we study daily areas of sunspot groups that are observed within $\pm 10^\circ$ central meridian distance. The data are taken from the US Air Force and US National Oceanic and Atmospheric Administration (USAF/NOAA), who regularly compile sunspot observations from different observatories. We note that this is only a rough check since we did not directly calculate the sunspot area within the considered $[-10^\circ, 10^\circ]$ central meridian slice (as we did for CHs) but summed the areas of all sunspot groups that had their center coordinate within the $\pm 10^\circ$ slice.

3. Method

Wavelet power spectra (WPS) are an appropriate tool for investigating time series that contain nonstationary power at many different frequencies (Daubechies, 1990). In particular, they can be used to determine predominant periods in a time series together with their times of appearance. We use the Morlet wavelet (Grossman and Morlet, 1984) as analyzing wavelet function $\psi(\tau)$, where τ is a nondimensional time parameter. The continuous wavelet transform can be written as

$$W_n(s) = \sum_{k=0}^{N-1} \hat{x}_k \hat{\psi}^*(s\omega_k) e^{i\omega_k n \delta t}, \tag{1}$$

with δt the equal spacing in time, N the number of data points in the time series $\{x_n\}$, $\hat{x}_k$ the discrete Fourier transform of x_n, and $\hat{\psi}^*(s\omega_k)$ the scaled and translated version of $\psi(\tau)$ (* indicates the complex conjugate). The angular frequency ω_k is defined as

$$\omega_k = \begin{cases} \dfrac{2\pi k}{N\delta t} & \text{for } k \le \dfrac{N}{2}, \\ -\dfrac{2\pi k}{N\delta t} & \text{for } k > \dfrac{N}{2}. \end{cases} \tag{2}$$

With the actual choice for the value of ω, one can specify either a high resolution in time or a high resolution in frequency. We have chosen the value $\omega = 12$ as a moderate value showing reasonable resolution in both frequency and time. All WPS presented in Section 4.1 were calculated for the time range 1 January 2005 to 11 September 2005 and for periods in the range 2 – 40 days. For the WPS in Section 4.2, the periods from 2 to 40 days are calculated for the entire time span of ACE data, *i.e.*, ~1998 – 2006. As significance tests, confidence levels at 80% and 95% are calculated by using a red noise background spectrum. Regions where edge effects become important, because of the finite length of the time series, are labeled as the cone of influence (COI). We further present the global wavelet spectrum (GWS), which is the time-averaged wavelet spectrum over a certain period (given in arbitrary units). The computation of all these parameters is performed in the way described by Torrence and Compo (1998).

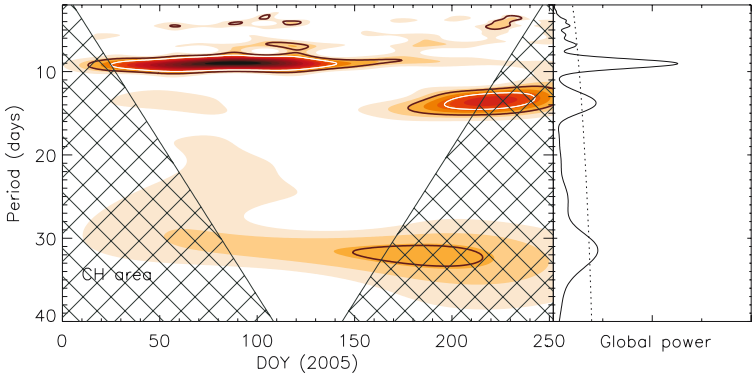

Figure 2 WPS (left) and GWS (right) from fractional areas of coronal holes for the analyzed time span 1 January 2005 until 11 September 2005, *i.e.*, DOY 1 – 254. Black (white) contour lines indicate significance levels of 80% (95%). The COI is indicated by cross-hatched regions. The dotted line in the GWS represents the 95% significance level.

4. Results

4.1. The Time Period 2005

In Figure 1 (bottom panel) daily values of fractional coronal hole areas for the analyzed time range are plotted. Within the period DOY 20 – 130 several periodically appearing distinct peaks are obtained. Calculating the WPS from this data set, we obtain a significant (95%) periodicity of 9 days for the time range DOY 20 – 140 (see Figure 2). The GWS in Figure 2 reveals four peaks above the 95% significance level, namely at periods of 9, 13.5, 31.5, and 7 days (ordered from the highest to the lowest power). Note that the peak at 9 days is by far the strongest one. During this time range, the SXI images clearly show a triangular distribution of large CHs, consisting of low-latitude CHs not connected to polar regions, as well as polar CHs (*cf.* animation of Figure 1). This configuration of large CHs, mutually separated from each other by $\sim$120° in longitude, is stable and recurs from DOY 20 until 120 (*cf.* animated Figure 1). In addition, a period of 7 days shows up in the WPS at about DOY 100 – 130, which can be identified in the SXI images as newly upcoming small-scale CHs in addition to the stable triangular pattern of large CHs. In the time range DOY 190 – 240, a distinct (significance level of 95%) period of 13.5 days is obvious from the WPS that was generated by two CHs situated roughly 180° apart—one of the CHs was extending from polar to equatorial regions, and another one was an isolated low-latitude CH. During DOY 150 – 210, the WPS shows enhanced power in the period range of 32 days, which is probably due to solar rotation of high-latitude CHs. However, we note that in the WPS this period is to a large extent covered by the COI.

Figure 3 presents the WPS and GWS for the solar wind parameters: velocity, density, temperature, and magnetic field magnitude (from top to bottom). The variations of all solar wind parameters studied seem to be correlated among each other and show similar variations in time. Enhanced power (>95% significance) of a 9-day period is obtained during the time span DOY 20/30 – 130/140, obviously matching the periodicity in CH areas (*cf.* Figure 2). Around DOY 120 the power evolves toward a 7-day period, similar to that obtained for the CH areas. After a short interception, the 9-day period returns during DOY 160 – 250 (partly covered by the COI), which has no correspondence with the periodic appearance of CHs.

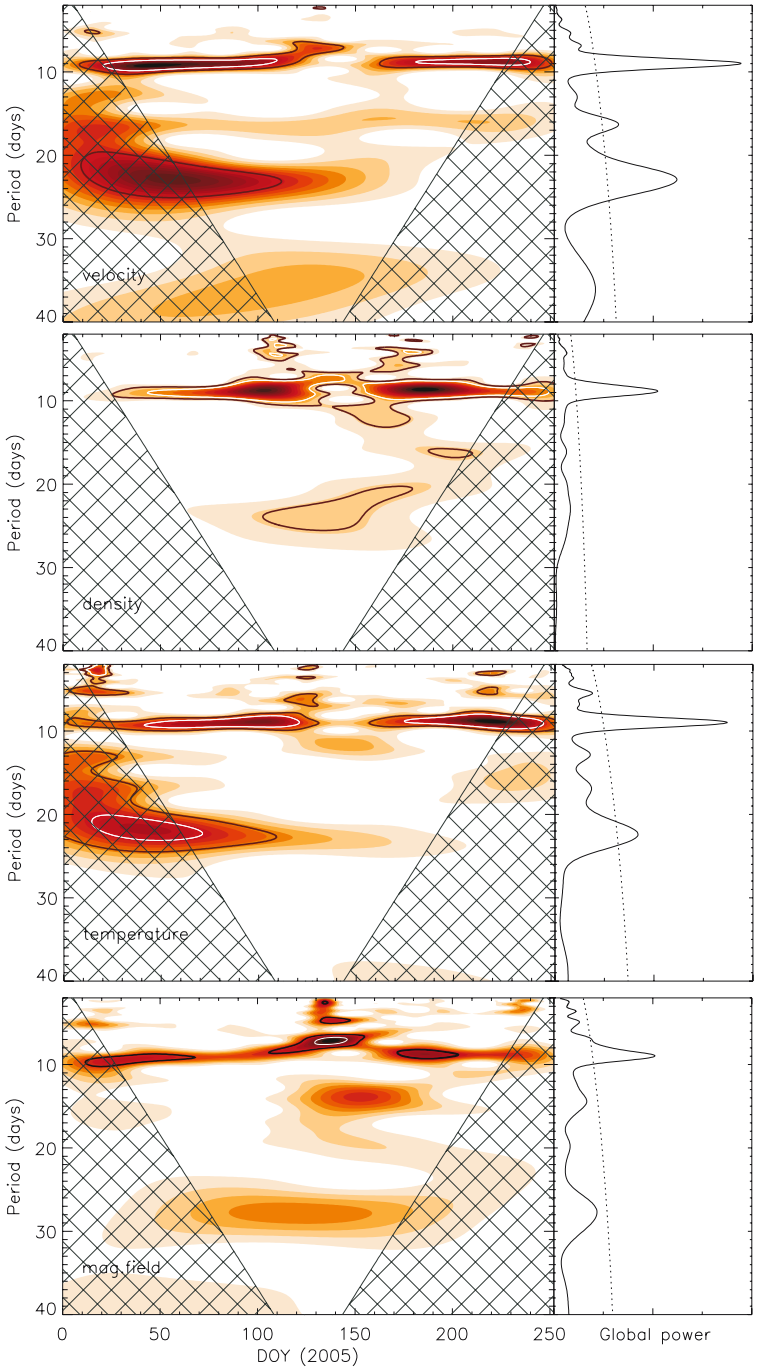

Figure 3 Same as Figure 2 but for the ACE solar wind parameters, from top to bottom: velocity, density, temperature, and magnetic field magnitude.

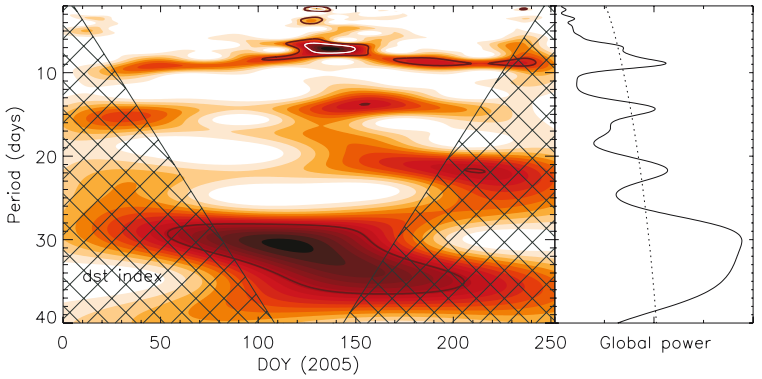

Figure 4 Same as Figure 2 but for the *Dst* index.

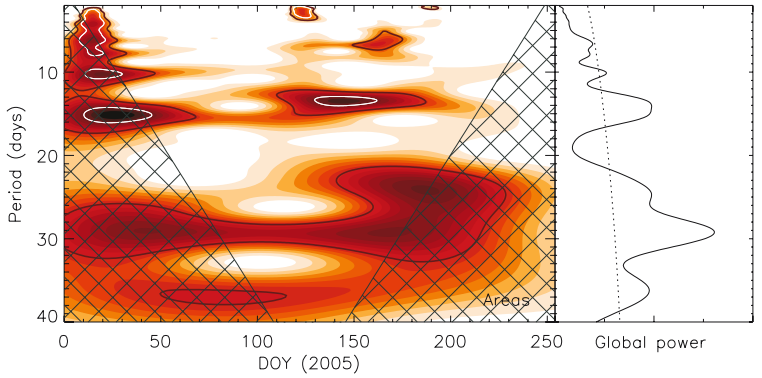

Figure 5 Same as Figure 2 but for the daily areas of sunspot groups within $\pm 10^{\circ}$ central meridian distance.

We note that the 9-day period is most pronounced in the solar wind velocity, density, and temperature and is less significant for the magnetic field variations. However, for each solar wind parameter, the strongest signal in the GWS is at a period of 9 days.

Figure 4 shows the WPS and GWS for the geomagnetic activity as quantified by the *Dst* index. The most eminent peak in the WPS is in the range of 7 days (DOY 120 – 150), but also the 9-day period is revealed with power above the 80% significance level from DOY 170 to 240. Further significant periods obtained are of 14.5 and 22 days. A broad power enhancement covering the periods from 29 to 33 days is seen from the WPS and GWS. Note that this power enhancement is partly covered by the COI.

Figure 5 shows the WPS and GWS from daily areas of sunspot groups with a central meridian distance of $\pm 10^{\circ}$. As can be seen, the highest power is revealed at $\sim$29 days; an increased power is also obtained at $\sim$14 days. There is no significant enhancement of power in the range of 9 days after DOY 25.

4.2. Periodicities in the Complete Set (1998 – 2006) of ACE Data

To compare the variability of solar wind and magnetic field parameters during different phases of cycle 23, we calculated the WPS and GWS for the full range of available ACE data, $\sim$1998 – 2006, *i.e.*, almost fully covering solar cycle 23.

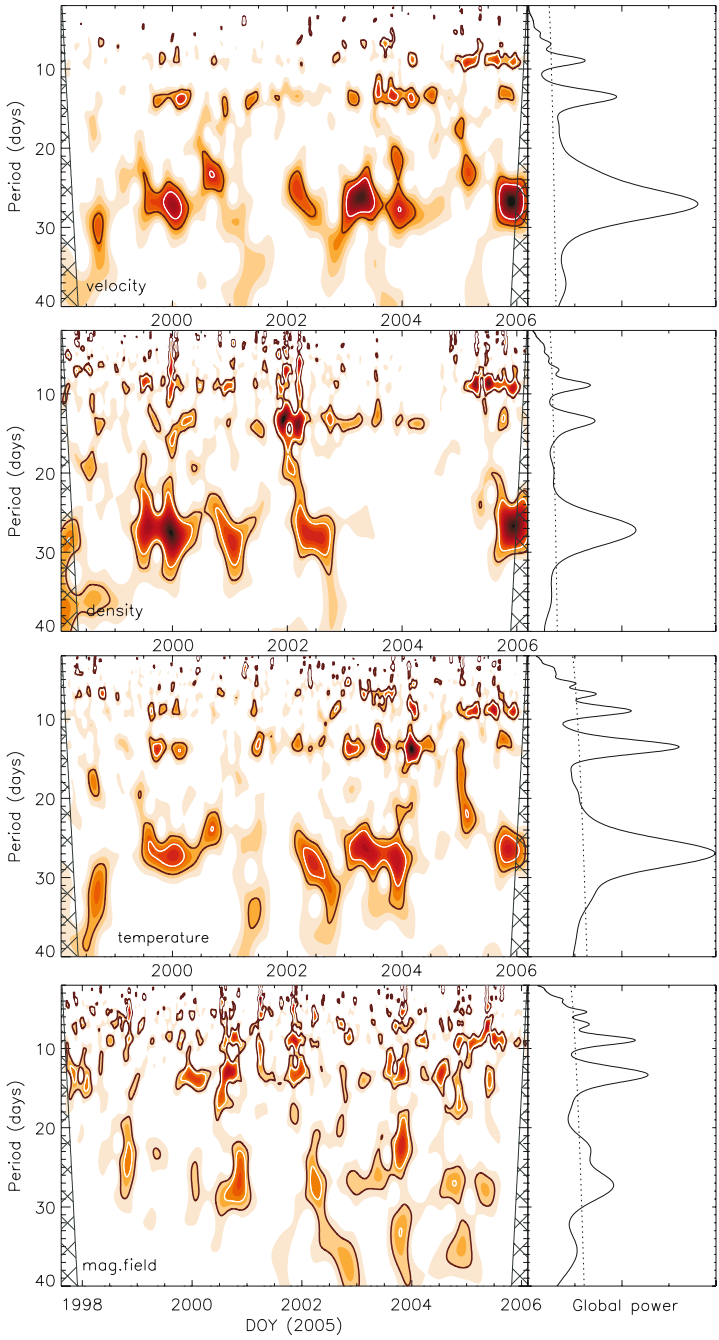

Figure 6 WPS (left) and GWS (right) from ACE data covering the period 4 February 1998 until 11 March 2006 (first three panels from top to bottom: velocity, density, temperature) and 1 September 1997 until 12 February 2006 (bottom panel: magnetic field magnitude). Black (white) contour lines indicate significance levels of 80% (95%), respectively. The COI is indicated by cross-hatched areas. The dotted line in the GWS represents the 95% significance level.

As can be seen from Figure 6, for the solar wind parameters velocity, density, and temperature, the ∼27-day period has the highest peak in the GWS but we obtain also high global power (above 95% significance) for the 13.5- and 9-day periods. The 9-day period is most pronounced when approaching the minimum phase of solar cycle 23 (2005); however, it is also present for the maximum (2000) and the declining phase (2002 – 2004). During the maximum and declining phase, the 9-day period shows up intermittently over no more than two solar rotations. Only during 2005 it can be tracked over 5 – 8 solar rotations (Figure 6, see also Section 4.1). The solar wind parameters show enhanced power for the 13.5-day period during the maximum phase around the year 2000 and even more distinct after 2003. For the magnetic field, the most significant periods are of 13.5 and 9 days (GWS), which reveal a very irregular pattern of enhanced power in the WPS over the cycle.

5. Discussion and Conclusion

We inspected and compared the variability of solar, heliospheric, and geomagnetic parameters to follow periodic patterns evolving from their source located on the Sun until their consequences at the Earth. We therefore combined statistical results from wavelet power spectra together with direct solar observations, which is essential for the correct interpretation of the statistical results.

The present study is based on the CH areas extracted from SXI images in the wavelength range 0.6 – 6 nm. Here the question arises as to what extent these values are comparable to the CH areas determined from observations in the He I 1083 nm wavelength. Studies on forecasting the solar wind speed based on CH areas extracted from He I 1083 nm spectroheliograms (Kitt Peak) by Robbins, Henney, and Harvey (2006) and SXI (same data as used in the present study) by Vršnak, Temmer, and Veronig (2007) led to almost the same results. From this we conclude that the areas extracted from SXI data are basically in conformity with those from He I observations, although there are differences in the determination of the CH boundaries (see de Toma and Arge, 2005; Shen *et al.*, 2006). For our purpose of a statistical analysis, this quantitative agreement is sufficient.

As can be seen from Figure 7 showing the daily number of CMEs as well as their average velocities $\langle v \rangle$ (summed velocity of daily observed CMEs divided by their number),[2] the time span 25 January 2005 until 5 May 2005, *i.e.*, DOY 25 – 125, is a period of very low CME activity (if one considers only geoeffective ones, *i.e.*, full halo and partial halo CMEs). Focusing on this time range, we found that periodic variations of 9 days originating from a distinct distribution of CHs are equally obtained in solar wind parameters. Such a behavior provides strong evidence that the periodicities in the solar wind parameters, showing up as higher harmonics of the solar rotation frequency, are generated by the "periodic" longitudinal distribution of CHs. After DOY 130 high CME activity starts and this may strongly disturb the "background" solar wind (shocks, density fluctuations, and rotating magnetic field) and destroy the direct relation between the variations of CH areas and solar wind parameters.

The inspection of daily areas of sunspot groups that occurred within the central meridian distance of $\pm 10^\circ$ revealed no distinct 9-day period for the same time range as observed for

[2]The data were taken from the CME online catalog and can be found under http://cdaw.gsfc.nasa.gov/CME_list/; detailed information on partial/full halo CMEs is given at http://lasco-www.nrl.navy.mil/halocme.html (*cf.* Yashiro, Gopalswamy, and Michalek, 2004).

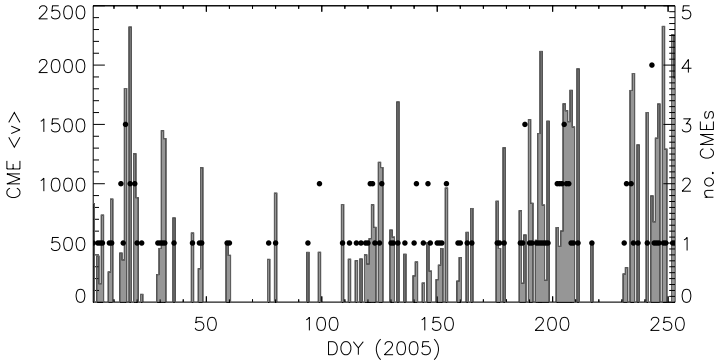

Figure 7 Daily number of CMEs (black dots) and their average velocity $\langle v \rangle$. Only partial (CMEs with widths between 120° and 359°) and full halo CMEs were extracted from the catalog.

CH areas and solar wind parameters. Although this is a rough check, we may exclude the association of distinct periodic variations observed in solar wind parameters with complexes of activity ("active longitudes") as suggested by Gaizauskas *et al.* (1983).

The periodic variations of CH areas is not replicated equally well for all solar wind parameters studied. The solar wind speed, temperature, and density reveal the most direct relation to the distribution and sizes of CHs. The solar wind magnetic field shows a somewhat less distinct correlation with the variation of CH areas, but it still follows the same pattern of periodicities (see also Vršnak, Temmer, and Veronig, 2007). The wavelet spectrum calculated for geomagnetic disturbances as quantified by the *Dst* index matches only weakly the spectral result from CH areas but is more similar to that of the magnetic field magnitude of the solar wind (compare the bottom panel of Figure 3 with Figure 4). This is to be expected since geomagnetic activity not only depends on fast solar wind streams emanating from CHs but relies on other factors, most importantly on the orientation of the interplanetary magnetic field with respect to Earth's magnetic field (Schwenn, 2006). Therefore, the relation to the structure of the solar corona is less direct for the *Dst* index than for the solar wind parameters.

The clear (triangular) distribution of CHs and their stable appearance over several solar rotations, which causes the distinct 9-day periodicity in the solar wind parameters, is related to the underlying large-scale patterns of the coronal magnetic field. As gathered from magnetic source surface extrapolations (see Wilcox Observatory under http://wso.stanford.edu/synsource.html), a similar pattern is seen to what we obtained for the triangular distribution of coronal holes. The observed large-scale distribution of the magnetic field may be related to downflow regions of "giant convective cells" (Bumba, 1987). The existence of giant cells was first suggested by Bumba and Howard (1965); however, their subsequent history was quite controversial (see also Hathaway, Beck, and Bogart, 2000). Indications were found for various solar activity phenomena during various solar cycles. For example, Vršnak, Pohjolainen, and Urpo (1992) found for the microwave low-temperature/brightness regions, during various periods within the years 1979 – 1982 and 1987 – 1989, large-scale patterns that were comparable with observed magnetic field distributions. Further evidence for a large-scale evolution/distribution of solar activity and the global magnetic field is given by Chertok (2001) from studying microwave, soft X-ray, and EUV emitting structures (chains) that seem to coincide with the boundaries of coronal holes.

From the entire ACE data set (∼1998 – 2006) we found that the occurrence of 9- and 13.5-day periods is not restricted to the declining phase of a solar cycle but can also be occasionally obtained during the maximum and close to the minimum phase of cycle 23, however, over much smaller time intervals. Similar results were obtained by Nayar *et al.* (2001), who analyzed solar wind and interplanetary magnetic field data from 1964 to 2000. These observational findings are partially in disagreement with the interpretation by Mursula and Zieger (1996), who supposed that a sufficiently flat and tilted heliosheet might generate two solar wind high-speed streams per one solar rotation, which subsequently produces a 13.5-day period in the solar wind parameters when the Earth encounters them. In this scenario, the 13.5-day period would only be expected at the minimum phase of a solar cycle.

Harvey and Recely (2002) describe an evolutionary process for CHs observed during solar cycles 22 and 23, in which isolated high-latitude CHs might be pre-polar CHs, evolving in time to polar CHs (after 5 – 8 solar rotations). Since polar CHs are stable and rigidly rotating objects, they may exist for several years. During their decaying phase the polar CHs form isolated lobes. This evolutionary process contributes considerably to the time variation of CH areas and configuration and is observed to be most outstanding during times of solar maximum and minimum (Harvey and Recely, 2002). This might explain the persistence of periodic variations in solar wind parameters over several solar rotations during the minimum and maximum phase of the solar cycle. However, in this respect we stress that the solar wind variations, *i.e.*, its patterns measured at Earth, are dependent on other processes too, *e.g.*, CME activity, which cannot be straightforwardly related to CH distributions.

Acknowledgements We thank the ACE SWEPAM and ACE MAG instrument teams and the ACE Science Center for providing the ACE data and the GOES-SXI, SoHO-LASCO, and WDC-Geomagnetism-Kyoto teams for their open data policies. M.T. gratefully acknowledges the Austrian *Fonds zur Förderung der wissenschaftlichen Forschung* (FWF Grant No. J2512-N02). This work is supported by the Air Force Office of Scientific Research, Air Force Material Command, USAF, under Grant No. FA8655-06-1-3036. We would like to thank the anonymous referee for helpful comments on the manuscript.

References

Alfvén, H.: 1977, *Rev. Geophys. Space Phys.* **15**, 271.
Altrock, R.C.: 2003, *Solar Phys.* **213**, 23.
Alves, M.V., Echer, E., Gonzalez, W.D.: 2006, *J. Geophys. Res.* **111**, 7.
Bartels, J.: 1940, *J. Geophys. Res.* **45**, 339.
Bobova, V.P., Stepanian, N.N.: 1994, *Solar Phys.* **152**, 291.
Bumba, V.: 1987, *Bull. Astron. Inst. Czechoslov.* **38**, 92.
Bumba, V., Howard, R.: 1965, *Astrophys. J.* **141**, 1502.
Chertok, I.M.: 2001, *Solar Phys.* **198**, 367.
Cliver, E.W., Ling, A.G.: 2001, *Astrophys. J.* **556**, 432.
Crooker, N.U., Cliver, E.W.: 1994, *J. Geophys. Res.* **99**, 23383.
Daubechies, I.: 1990, *IEEE Trans. Inf. Theory* **36**, 961.
de Toma, G.D., Arge, C.N.: 2005, *ASP Conf. Ser.* **346**, 251.
Fisk, L.A.: 2005, *Astrophys. J.* **626**, 563.
Gaizauskas, V., Harvey, K.L., Harvey, J.W., Zwaan, C.: 1983, *Astrophys. J.* **265**, 1056.
Gonzalez, W.D., Joselyn, J.A., Kamide, Y., *et al.*: 1994, *J. Geophys. Res.* **99**, 5771.
Gosling, J.T., McComas, D.J., Phillips, J.L., Bame, S.J.: 1991, *J. Geophys. Res.* **96**, 7831.
Grossman, A., Morlet, J.: 1984, *SIAM J. Math.* **15**, 723.
Harvey, K.L., Recely, F.: 2002, *Solar Phys.* **211**, 31.
Hathaway, D.H., Beck, J.G., Bogart, R.S., *et al.*: 2000, *Solar Phys.* **193**, 299.
Hill, S.M., Pizzo, V.J., Balch, C.C., *et al.*: 2005, *Solar Phys.* **226**, 255.
Hoeksema, J.T.: 1995, *Space Sci. Rev.* **72**, 137.

Hoeksema, J.T., Scherrer, P.H.: 1987, *Astrophys. J.* **318**, 428.
Hoeksema, J.T., Wilcox, J.M., Scherrer, P.H.: 1982, *J. Geophys. Res.* **87**, 10331.
Krieger, A.S., Timothy, A.F., Roelof, E.C.: 1973, *Solar Phys.* **29**, 505.
Leer, E., Holzer, T.E., Fla, T.: 1982, *Space Sci. Rev.* **33**, 161.
McComas, D.J., Bame, S.J., Barker, P.: 1998, *Space Sci. Rev.* **86**, 563.
Mursula, K., Zieger, B.: 1996, *J. Geophys. Res.* **101**, 27077.
Nash, A.G., Sheeley, N.R. Jr., Wang, Y.-M.: 1988, *Solar Phys.* **117**, 359.
Nayar, S.R., Sanalkumaran Nair, V., Radhika, V.N., Revathy, K.: 2001, *Solar Phys.* **201**, 405.
Neugebauer, M., Smith, E.J., Ruzmaikin, A., Feynman, J., Vaughan, A.H.: 2000, *J. Geophys. Res.* **105**, 2315.
Robbins, S., Henney, C.J., Harvey, J.W.: 2006, *Solar Phys.* **233**, 265.
Schwenn, R.: 1983, *Space Sci. Rev.* **34**, 85.
Schwenn, R.: 2006, *Living Rev. Solar Phys.* **3**, 2.
Schwenn, R., dal Lago, A., Huttunen, E., Gonzalez, W.D.: 2005, *Ann. Geophys.* **23**, 1033.
Shen, C., Wang, Y., Ye, P., Wang, S.: 2006, *Astrophys. J.* **639**, 510.
Smith, C.W., L'Heureux, J., Ness, N.F., *et al.*: 1998, *Space Sci. Rev.* **86**, 613.
Stone, E.C., Frandsen, A.M., Mewaldt, R.A., *et al.*: 1998, *Space Sci. Rev.* **86**, 1.
Sugiura, M., Chapman, S.: 1960, *Abh. Akad. Wiss. Göttingen* **4**, K1.
Sugiura, M., Wilson, C.R.: 1964, *J. Geophys. Res.* **69**, 1211.
Svalgaard, L., Wilcox, J.M.: 1975, *Solar Phys.* **41**, 461.
Torrence, C., Compo, G.P.: 1998, *Bull. Am. Meteor. Soc.* **79**(1), 61.
Tsurutani, B.T., Gonzalez, W.D.: 1987, *Planet. Space Sci.* **35**, 405.
Tsurutani, B.T., Gonzalez, W.D.: 1997. In: Tsurutani, B.T., *et al.* (eds.) Geophys. Monograph Series **98**, American Geophysical Union, Washington, 77.
Tsurutani, B.T., Gonzalez, W.D., Guarnieri, F., *et al.*: 2004, *J. Atmos. Solar-Terr. Phys.* **66**, 167.
Vršnak, B., Pohjolainen, S., Urpo, S., *et al.*: 1992, *Solar Phys.* **137**, 67.
Vršnak, B., Temmer, M., Veronig, A.: 2007, *Solar Phys.*, in press.
Wang, Y.-M., Sheeley, N.R. Jr.: 1993, *Astrophys. J.* **414**, 916.
Yashiro, S., Gopalswamy, N., Michalek, G., *et al.*: 2004, *J. Geophys. Res.* **109**, 7105.
Zhang, J., Dere, K.P., Howard, R.A., Bothmer, V.: 2003, *Astrophys. J.* **582**, 520.